Supporting Information for

Development of a Trajectory Model for Predicting Attachment of Submicrometer Particles in Porous Media: Stabilized NZVI as a Case Study

Yu-Ting Wei and Shian-chee Wu*

Graduate Institute of Environmental Engineering

National Taiwan University

71 Chou-Shan Rd., Taipei 106, Taiwan, R. O. C.

* Corresponding author phone: +886-2-2362-9435; fax:

+886-2-2362-9435; e-mail: scwu@ntu.edu.tw

The Flow Field of Constricted Tube Applied to the Simulation

A two-dimensional flow field equation established by Chow and Soda (*1*) is adopted

for our simulation. Their analytical solution of the steady laminar flow of an

impressible Newtonian fluid in an axisymmetric sinusoidal constricted tube is suitable

for simulating the groundwater environment. However, the stream function (ψ) for

zero-order term of velocity component along the r direction was mistyped. The

following lists the corrected equations of stream function and velocity components.

Stream function:

Zero-order:

$$\psi_0 = \frac{1}{2}(R^4 - 2R^2) = \frac{1}{2}G \tag{S1}$$

First-order:

$$\psi_1 = \left[\left(\frac{1}{4}\mathrm{Re}\,\omega\frac{dg}{dz}\right)/\eta\right]f(R) \tag{S2}$$

Second-order:

$$\psi_2 = -\frac{1}{2}\omega\left[5\omega\left(\frac{dg}{dz}\right)^2 - \eta\frac{d^2g}{dz^2}\right]K(R) - \left[\frac{1}{8}\mathrm{Re}^2\,\omega^2\left(\frac{dg}{dz}\right)^2/\eta^2\right]F(R) \tag{S3}$$

where $R = r/r_w$, $\omega = (r_{max} - r_c)/(r_{max} + r_c)$, $g = \cos(2\pi\frac{z}{h})$, $\eta = r_w/r_m$ in this study,

Re is the Reynolds number.

$$f(R) = \frac{1}{9}(R^8 - 6R^6 + 9R^4 - 4R^2) \tag{S4}$$

$$K = (R^2 - 1)^2 R^2/3 \tag{S5}$$

$$F = (1/3600)(32R^{12} - 305R^{10} + 750R^8 - 713R^6 + 236R^4) \tag{S6}$$

Velocity components:

r-direction

$$\frac{v_r}{<U_0>} = -\frac{1}{2\eta^2 R}\frac{dG}{dR} - \frac{\varsigma\omega\mathrm{Re}}{4\eta^3 R}\frac{dg}{dz}\frac{df}{dR} - \frac{\varsigma^2}{\eta^2 R}\frac{\partial\psi_2}{\partial R}$$ (S7)

z-direction

$$\frac{v_z}{<U_0>} = -\frac{\varsigma\omega}{2\eta^2}\frac{dg}{dz}\frac{dG}{dR} + \frac{\varsigma^2\omega}{4\eta^3}\left\{\left[\varsigma\frac{d^2g}{dz^2} - \omega\left(\frac{dg}{dz}\right)^2\right]\right\}Rf - \mathrm{Re}\,\omega\left(\frac{dg}{dz}\right)^2\frac{df}{dR}$$
$$+\frac{\varsigma^3}{\eta}\left(\frac{\partial\psi_2}{R\partial z} - \frac{\omega}{\eta}\frac{dg}{dz}\frac{\partial\psi_2}{\partial R}\right)$$ (S8)

where $\varsigma = r_m / h$ in this study

$$\frac{\partial\psi_2}{\partial R} = -\frac{\omega}{2}\left[5\omega\left(\frac{dg}{dz}\right)^2 - \eta\frac{d^2g}{dz^2}\right]\frac{dK}{dR} - \frac{\mathrm{Re}^2\,\omega^2}{8}\left(\frac{1}{\eta}\frac{dg}{dz}\right)^2\frac{dF}{dR}$$ (S9)

$$\frac{\partial\psi_2}{\partial z} = -\frac{\omega}{2}\left(9\omega\frac{dg}{dz}\frac{d^2g}{dz^2} - \eta\frac{d^3g}{dz^3}\right)K - \frac{\mathrm{Re}^2\,\omega^2}{8\eta^2}\left[2\frac{dg}{dz}\frac{d^2g}{dz^2} - 2\frac{\omega}{\eta}\left(\frac{dg}{dz}\right)^3\right]F$$ (S10)

$<U_0>$ is the average axial velocity.

$$<U_0> = \frac{U}{N_c\pi r_m^2}$$ (S11)

U is the approach (superficial) velocity. N_c is the total number of the

constricted tubes present in an UBE (2). r_m is the average tube radius.

$$N_c = \frac{3\varepsilon(1-S_w)}{2\pi r_c^2}\left[\frac{8(1-\varepsilon)r_c^3}{\varepsilon(1-S_w)d_g^3}\right]^{2/3}$$ (S12)

where ε is the porosity, S_w is the fraction of irreducible saturation (3) (S_w =

0.127 in this study), d_g is the filter-grain diameter.

The Universal Functions for Hydrodynamic Retardation Correction of the Drag and Brownian Forces

The universal functions for hydrodynamic retardation correction of the drag and Brownian forces were presented by Elimelech (*4*). The approximation of universal functions from Adamczyk et al. (*5*) was adopted for calculating f_1, f_2, f_3 and f_4 as following

$$f_1 = \frac{19H^2 + 4H}{19H^2 + 26H + 4} \tag{S13}$$

$$f_2 = 1 + \frac{1.79}{\left(0.828 + H\right)^{1.167}} \tag{S14}$$

$$f_3 = \frac{1}{0.754 - 0.256\ln(H)} \quad , H < 0.137 \tag{S15}$$

$$f_3 = 1 - \frac{0.304}{(1+H)^3} \quad , H \geq 0.137$$

$$f_4 = \frac{1}{1.062 - 0.516\ln(H)} \quad , H < 0.11 \tag{S16}$$

$$f_4 = \left(\frac{H}{2.639 + H}\right)^{1/4} \quad , H \geq 0.11$$

The expressions of two random deviates, R_u and R_x accounted for the effect of Brownian force

$$R_u = \sigma_c \sigma_u N_1 + \sigma_{u|x} N_2 \qquad\qquad (S17)$$

$$R_x = \sigma_x N_1 \qquad\qquad (S18)$$

where $\sigma_c = \alpha \beta_0^{-2} \left(1 - e^{-\beta_0 \Delta t}\right)^2 / \left(\sigma_u \sigma_x\right)$, $\sigma_u = \left[\alpha \beta_0^{-1} \left(1 - e^{-2\beta_0 \Delta t}\right)\right]^{1/2}$,

$\sigma_x = \left[\alpha \beta_0^{-3} \left(2\beta_0 \Delta t - 3 + 4e^{-\beta_0 \Delta t} - e^{-2\beta_0 \Delta t}\right)\right]^{1/2}$, $\sigma_{u|x} = \sigma_u \left(1 - \sigma_c^{\,2}\right)^{1/2}$, $\alpha = \beta_0 kT / m_p$,

N_1 and N_2 are two Gaussian random numbers with zero mean and unit variance. As the hydrodynamic retardation effect is direction dependent, normal ($R_{u\perp}$ and $R_{x\perp}$) and tangential ($R_{u\|}$ and $R_{x\|}$) components of R_u and R_x are presented separately by adjusting β_0 value as $\beta_\perp$ ($=\beta c_s / f_1$) for $R_{u\perp}$ and $R_{x\perp}$, and $\beta_\|$ ($=\beta c_s / f_4$) for $R_{u\|}$ and $R_{x\|}$.

The computational algorithm

The computational flow chart of the Fortran program is shown in Figure S1, with the step-by-step calculating process related to applied equations given below:

1. Assigning initial position to particle and calculating the initial velocities

   The probability of collection was computed from the initial location at 0.99 ($r_{max} - a_p$) down to the origin of the center of the constricted tube. The computation of the initial velocities were derived from eq 3 and eq 4, and required

three additional parameters, wall radius (r_w), total number of the constricted tubes, (N_c), and average axial velocity, ($<U_0>$). The initial location was applied in eq 1 to calculate the wall radius, r_w. The total number of the constricted tubes, N_c, present in an UBE was from eq S12 then N_c was applied in eq S11 to calculate the average axial velocity, $<U_0>$.

2. Translating and rotating the coordinates

It should be noted that universal functions (eq S13 – eq S16) are only effective on normal and tangential direction between the particle and tube surface. However, velocity components derived from analytical solution are along the r and z direction. Thus, when simulating the particle trajectory, the translation and rotation of coordinates are necessary to calculate the trajectory during each time step interval. Translation depends on the position of particle in r-z coordinate system. Rotation uses angle θ formed by z-axis and the tangent to the tube surface at point O''. θ is negative when z < h and positive when z > h. The r-z coordinate system is translated first, then rotated by $-\pi/2+\theta$ to become normal and tangential to tube surface coordinates.

3. Calculating position and velocity components including force and random Brownian motion

To compute particle position components, initial positions and velocities

calculated in step 1, universal functions (eq S13 – eq S16), the forces (eq 2), and

the random Brownian motion deviates (eq S17 and S18) are all applied in eq 5 and

eq 6. To compute particle velocity components, the abovementioned parameters

less initial positions are all applied in eq 3 and eq 4.

4. Calculating the new particle position and velocity components after each step time

    interval

    To compute the new particle position components after each step time interval,

    positions and velocities calculated, along with parameters in step 2, are all applied

    in eq 5 and eq 6. To compute new particle velocity components, velocities

    calculated and the abovementioned parameters in step 2 are all applied in eq 3 and

    eq 4.

5. Determining if the particle is collected or eluted

    If the separation distance is less than $5\overset{\circ}{A}$ (the same as used in reference 6) after

    iterating step 3 and step 4, the particle is determined as collected. If the

    z-direction position of particle is greater than the grain diameter, the particle is

    determined as eluted. The other particles were determined to be either collected or

    eluted by following the above steps until all particles were realized for the

    assigned initial position. The probability of collection at the initial location was

    determined by calculating the ratio of collected particles.

6. Calculating the collection efficiency of a specific particle size

The probability of collection was computed from the initial location at 0.99 $(r_{max} - a_p)$ down to the origin of the center of the constricted tube. If the probability of collection was zero for the location, we assumed that the probabilities of collection computed from the next other locations were all zero (outside the limiting trajectory) so that the initial locations required to be computed would be less than one hundred. Eq 8 then was used to calculate the total collection efficiency by summarizing the probability of collection efficiency of limiting trajectory.

The number of trajectory realizations

The total number of realizations used to compute the probabilities of collection for Figure 2 is listed in Table S1 for the reference. To access the effect of the number realizations, one convergence test of trajectory simulations is presented in Figure S2. In Figure S2, one realization equals one full set of trajectories from each starting location.

The parameter values used in experimental data simulation

All parameter values used in our simulation and experimental data are listed in Table S2. The parameters applied in Case 2 and Case 4 were directly adopted from measurements and references under the similar conditions. Some of the parameters applied in Case 1 were cited from measurements, with three parameters in steric force calculation derived from reference. In Case 3, the distance between the chain anchoring points is the only fitting parameter, with Hamaker constant and compressed thickness as the two assumed parameters, because there was no reported value of these parameters.

The breakthrough column test of a nonionic surfactant modified NZVI

Manufacturing of NZVI. One-hundred milliliters of ferrous sulfate solution ($FeSO_4 \cdot 7H_2O$, Merck, analytical) were slowly added into 100 milliliter of sodium boronhydrate ($NaBH_4$, Riedel-de Haëne, analytical) solution with continuous stirring. A nonionic surfactant was added into the solution two minutes after being added ferrous sulfate. The solution was degassed by sonication till there was no hydrogen ebullition.　The suspension was left standing for a period of time, and the supernatant was sampled for the analysis of NZVI. The size distribution of synthesized nanoparticles was measured by ZetaSizer instrument (3000HS, Malvern).

Soil Column Experiments. Alluvial soil taken from a CAHs contaminated site was air dried and sieved. Particles smaller than sieve opening of 0.3 mm (sieve #50) were collected then packed in a glass column with a diameter of 5 cm. The total height of soil layer is 30 cm. The porosity of soil is 0.483. After the column was conditioned with surfactant for one pore volume, nano-scale iron suspension was delivered into soil column with a hand-crank peristaltic metering pump from the lower end at linear velocity of 0.0053 cm/sec. Suspension from the higher end of the column was collected at different times for the analyses of iron concentration of NZVI.

In this study, total dissolved iron was detected by adding ascorbic acid (1% w/v) to the reaction mixture with ferrozine (3-(2-pyridyl)-5,6-bis (4-phenylsulfonic acid)-1,2,4-triazine). The reaction pH was buffered at 4.0 using acetic acid. In a FIA system (FS 3100, OI Corporation), a 0.1% nitric acid carrier carried the sample from the injection sample loop to the mixing tee, where the sample, carrier, and color reagent were mixed and the complex forming reaction began. The mixture moved through the reaction coil where the reaction proceeds to completion. The amount of colored complex was measured by using the absorbance detector (wavelength 540 nm) with the signal recorded and processed with an integrator. Total organic carbon was

measured by TOC detector (TOC 101, OI Corporation) to represent the concentration of surfactant.

Since the ionic strength was not controlled in manufacturing NZVI suspension, Russell approximation (*14*) was adopted to estimate ionic strength from conductivity. Conductivity was measured at 5000 μ mho/cm, which was converted to 0.08M of ionic strength.

Stability of Synthesized Nanoparticles. The stability of NZVI in the aqueous phase with different concentration of modifier was tested in batch type reaction. The suspension was left standing for 30 minutes, and the supernatant was sampled for the analysis of NZVI. The stability is defined as R (%) = iron concentration in supernatant / total iron concentration. The results show that applying nonionic surfactant at 5000 mg/L could keep stability at R= 94.74 %, which is better than R = 19.92 % at 500 mg/L and R = 31.78 % at 2500 mg/L of nonionic surfactant.

Size Distribution of Synthesized Nanoparticles. The size distribution of surfactant modified NZVI suspension is shown in Figure S3a. Most of the nanoparticle sizes are between 300 nm to 600 nm. The average size is about 400 nm. Compared with the size distribution of the surfactant-only suspension shown in Figure S3b, the NZVI particles seem to become larger due to forming aggregation of micelles.

Transport of Nano-scale Iron in Soil Column. The surfactant modified NZVI suspension with iron concentration at 1191.5 mg/L was injected in the soil column. The breakthrough curve of the concentration of NZVI is shown in Figure S4. After the peak concentration came out at about one pore volume, the breakthrough curve tailed and lasted for one half of a pore volume. The column outlet normalized particle concentration at the initial stage of the particle breakthrough curve is about 78%.

From our study, we found that the combination of the application of the nonionic surfactant was able to improve the transport of NZVI through porous media. The same surfactant applied in the field study was also proved to have the capability to enhance NZVI mobility (*15*). By employing the colloid filtration theory, the experimental results further illustrated that the nonionic surfactant was able to enhance the transport of NZVI in subsurface porous media.

The breakthrough column test of Poly(acrylic acid) (PAA) modified NZVI (*7*)

Soil Column Experiments. Alluvial soil taken from a CAHs contaminated site was air dried and sieved. Particles smaller than sieve opening of 0.3 mm (sieve #50) were collected then packed in a glass column with a diameter of 5 cm. The total height of soil layer is 10 cm. The porosity of soil is 0.48. 2500 mg/L Nano-scale iron suspension with 2500 mg/L PAA concentration, and was delivered into soil

column with a hand-crank peristaltic metering pump from the lower end at linear velocity of 0.0883 cm/sec. Suspension from the higher end of the column was collected at different times for the analyses of iron concentration of NZVI. In this study, total dissolved iron was detected by the same method as mentioned above. The conductivity was measured at 3500 μ mho/cm, which was converted to be 0.056M of ionic strength.

Size Distribution of Synthesized Nanoparticles. The size distribution of PAA modified NZVI suspension is shown in Figure S5. Most of the nanoparticle sizes are between 60 nm to 110 nm. The average size is about 100 nm.

Transport of Nano-scale Iron in Soil Column. The breakthrough curve of the concentration of NZVI is shown in Figure S6. After the peak concentration came out at about one pore volume, the breakthrough curve tailed and lasted for one half of a pore volume. The column outlet normalized particle concentration at the initial stage of the particle breakthrough curve is about 75%.

The modeling approach for calculating the total energy between material coated particle surface and collector surface

A simplified model (as shown in Figure S7) is used to calculate the net force between modified particle surface and collector surface. The model can be envisioned as a particular case of Ohshima's soft particle theory (*16*) with the assumption that the

softness parameter is so small that the polymer and surfactant coated particle behaves like a rigid particle and the slipping plane is positioned outward from bare particle surface to near the interface of bulk liquid and coated material. The potential on this new slipping plane becomes the zeta potential. The hydrodynamic radius measured by dynamic light scattering method (e.g. zetasizer) is adopted as the radius of effective hard particle used to simulate the collection efficiency because it is the apparent radius of the moving assembly of the bare particle and tightly covered polymer layer. Under such simplified assumption, we could apply the measured zeta potential to calculate the electrostatic force. The polymer layers show a concentration decrease near the outer boundary with an exponential fall or a cube root fall (*17*). When the polymer boundary and collector surfaces come close together, the polymer boundary on the surfaces may prevent them from coming into further closer. The apparent point of zero surface separation, therefore, corresponds to a real separation of 2δ (twice the thickness of the compressed polymer) while calculating the steric force (see the denominator of the term in parentheses in equation F_E in Table 1). Thus, equation F_E, applied to calculate the steric force, does not give a barrier, which is usually known to prevent primary minimum.

TABLE S1. Total Number of Realizations Applied for the Trajectory Simulation in Figure 2a, 2b, 2c

Particle size (μm)	Figure 2a	Figure 2b	Figure 2c
0.01	2500	4100	7100
0.02	2200	3600	5100
0.04	1900	2900	5100
0.10	1400	2500	3500
0.20	1100	2100	3200
0.35	1000	1800	2600
0.626	800	1500	2000
1.008	700	1200	1600
1.39	600	1100	1600
1.772	600	1000	1700
2.154	600	1100	1600
4	600	900	1500
6	600	1000	1700
8	600	1100	1800
10	600	1200	2100

Total number of realization = number of start locations×100 realizations/start location; e.g. in Figure 2a at particle size 0.01μm, total number = 25×100 = 2500

TABLE S2. Experimental Parameters Used in Applying the Trajectory Simulation

	Case 1	Case 2	Case 3	Case 4
modifier	PAA	PAA	PSS	nonionic surfactant
average molecular weight	2,000	2,000	70,000	--
references	SI, (7)	(8)	(9), (10)	SI
column flow direction	up-flow	down-flow	up-flow	up-flow
column length	10 cm	13 cm	25.5 cm	30 cm
C/C_0	0.75	0.6	0.9	0.78
particle diameter, d_p	0.1 μm	0.1 μm	0.05 μm	0.4 μm
grain diameter, d_g	0.3 μm	0.3 μm	0.3 μm	0.3 μm
approach velocity, U	8.83×10^{-4} m/sec	3×10^{-3} m/sec	3.2×10^{-4} m/sec	5.3×10^{-5} m/sec
porosity, ε	0.48	0.42	0.33	0.483
particle density, ρ_p	7.28 g/cm^3	7 g/cm^3	7.28 g/cm^3	1.3 g/cm^3
fluid density, ρ_f	1.0025 g/cm^3	1.0025 g/cm^3	1.0025 g/cm^3	1.02 g/cm^3
fluid viscosity, μ	1×10^{-3} kg/m/sec	1×10^{-3} kg/m/sec	1×10^{-3} kg/m/sec	8.9×10^{-4} kg/m/sec
Hamaker constant, A	8×10^{-20} J [a]	8×10^{-20} J [a]	6×10^{-20} J [b]	9×10^{-21} J [c]
ionic strength	0.056 M	0.01 M	0.01 M	0.08 M
zeta potential, ζ	-47.8 mV	-30 mV	-1 mV	-22.8 mV
reciprocal Debye length, κ	0.7888 nm^{-1}	0.3333 nm^{-1}	0.3333 nm^{-1}	0.9428 nm^{-1}
distance between the chain anchoring points, s	13.25 nm [d]	14.9 nm [d]	69 nm [e]	--
polymer end-to-end distance, L	9.3 nm [d]	11 nm [d]	75 nm	--
compressed thickness, δ	1.3 nm [d]	1.4 nm [d]	3.2 nm [b]	--

[a] Data refers to reference 11.

[b] The parameters are assumed.

[c] The parameter is assumed base on reference 12.

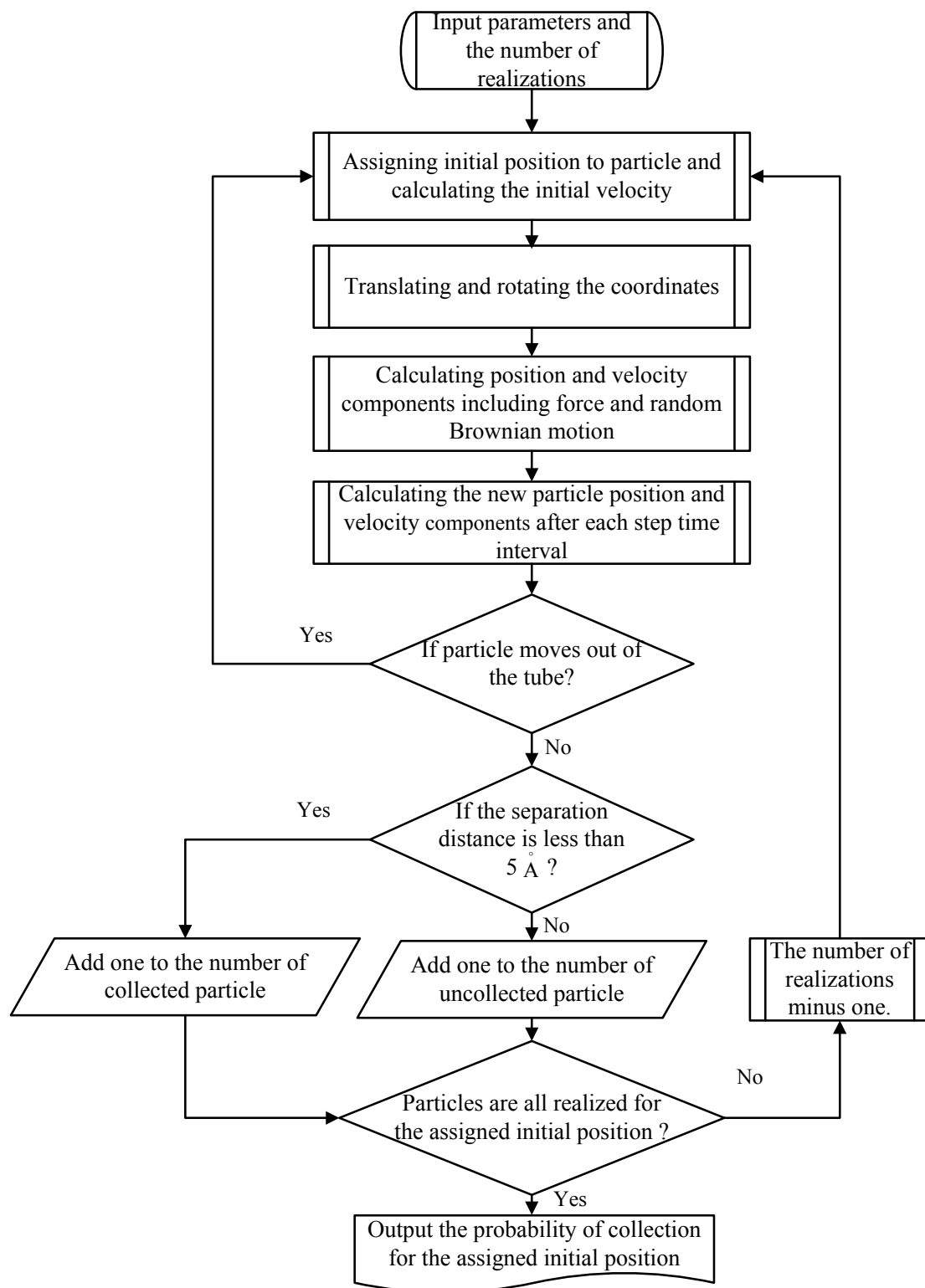[d] Data refers to reference 13.

[e] Data is a fitting value.

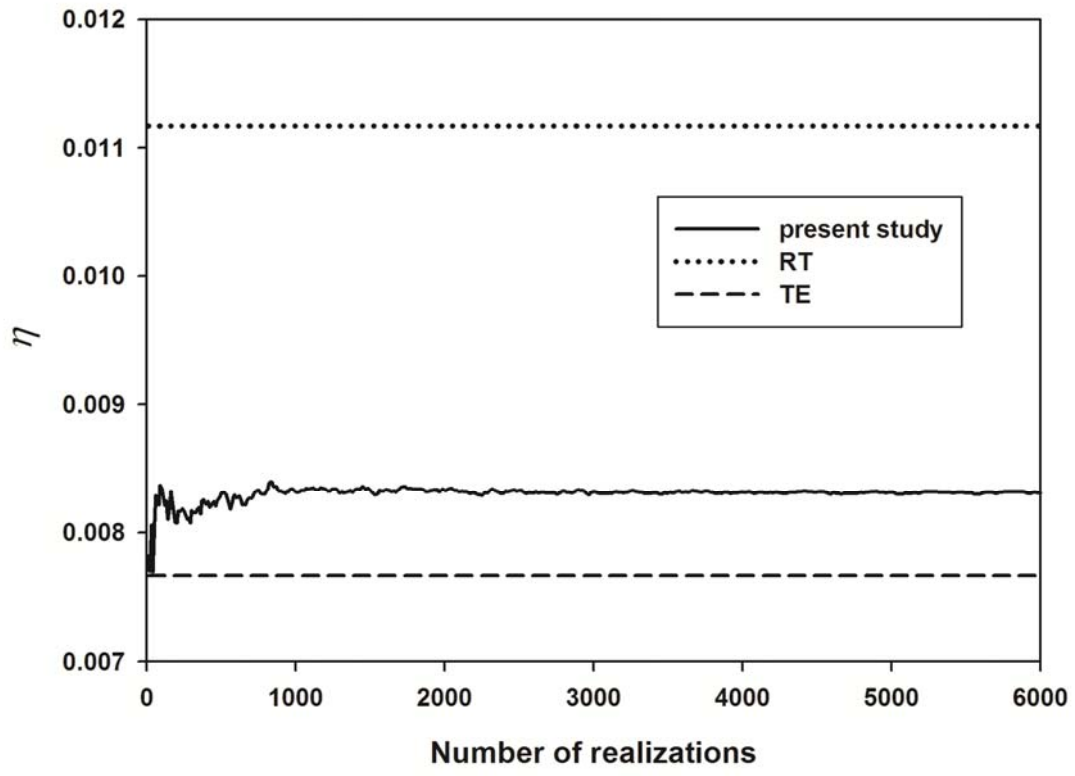FIGURE S1. The computational flow chart of the Fortran program applied to simulation.

FIGURE S2. Convergence test of trajectory simulations in present study. Parameters:

$a_p = 0.1\,\mu m,\ a_c = 163.5\,\mu m, \varepsilon = 0.372, U = 3.4375 \times 10^{-4}\ m/s, \Delta t = 1\,\mu\sec$. One

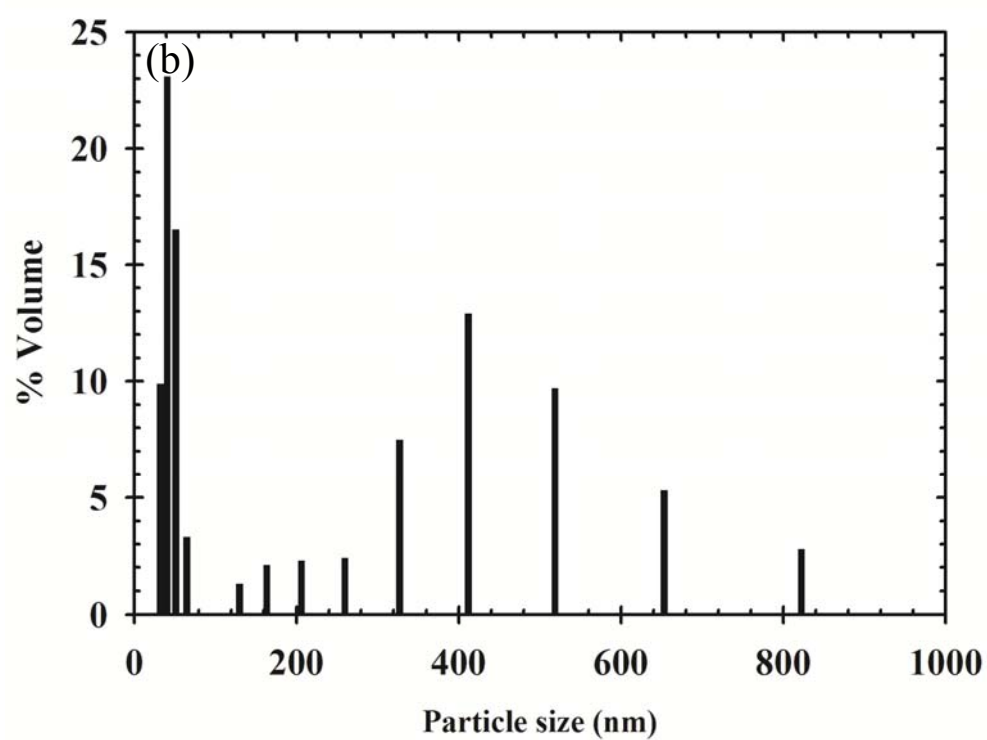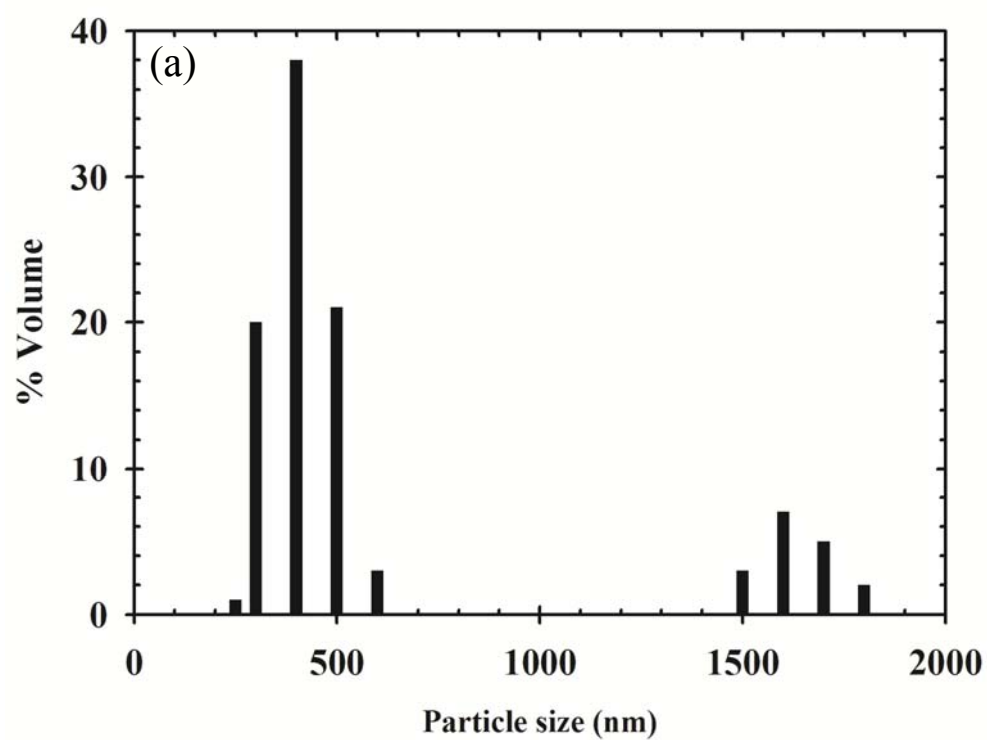realization equals one full set of trajectories from each starting location.

FIGURE S3. Volume-averaged particle size distribution fraction of (a) nonionic surfactant modified NZVI and (b) nonionic surfactant-only suspension.
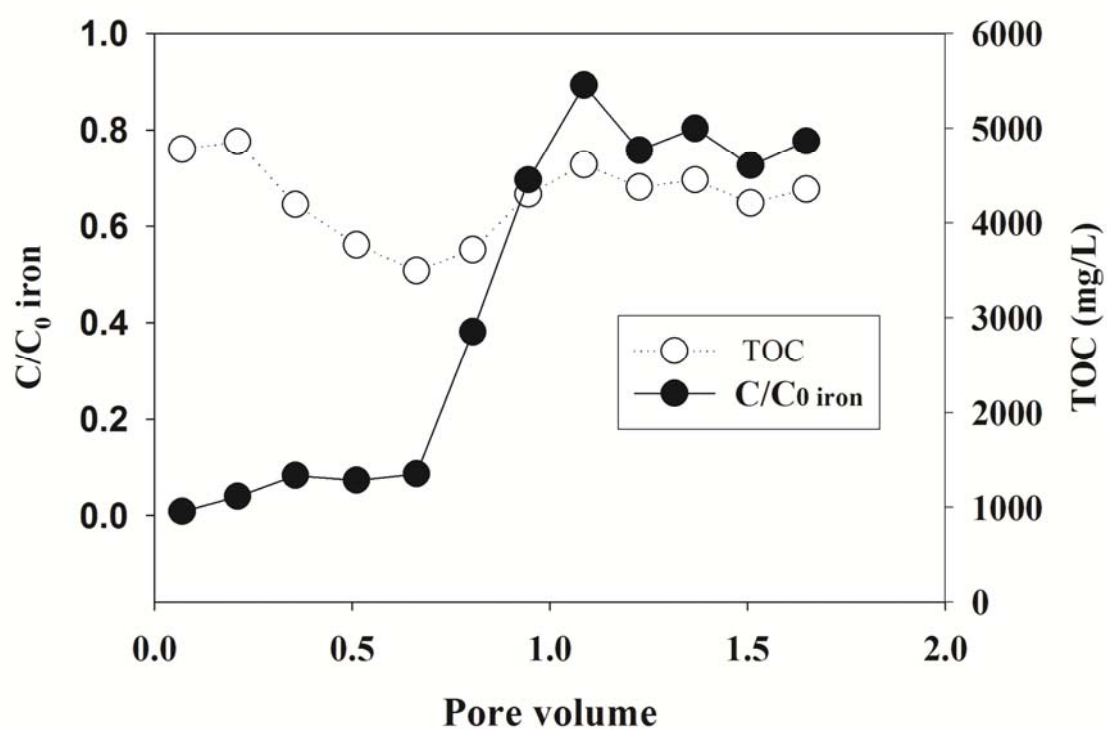
FIGURE S4. The eluted concentration of nonionic surfactant modified NZVI and total
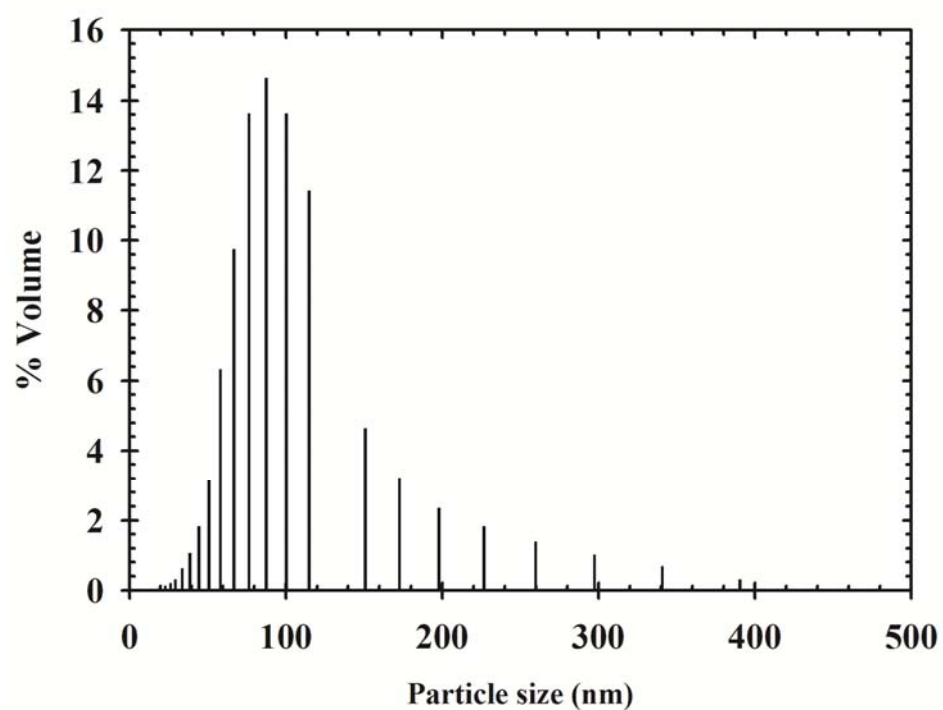
organic carbon (TOC) from the soil column.

FIGURE S5. Volume-averaged particle size distribution fraction of PAA modified NZVI.
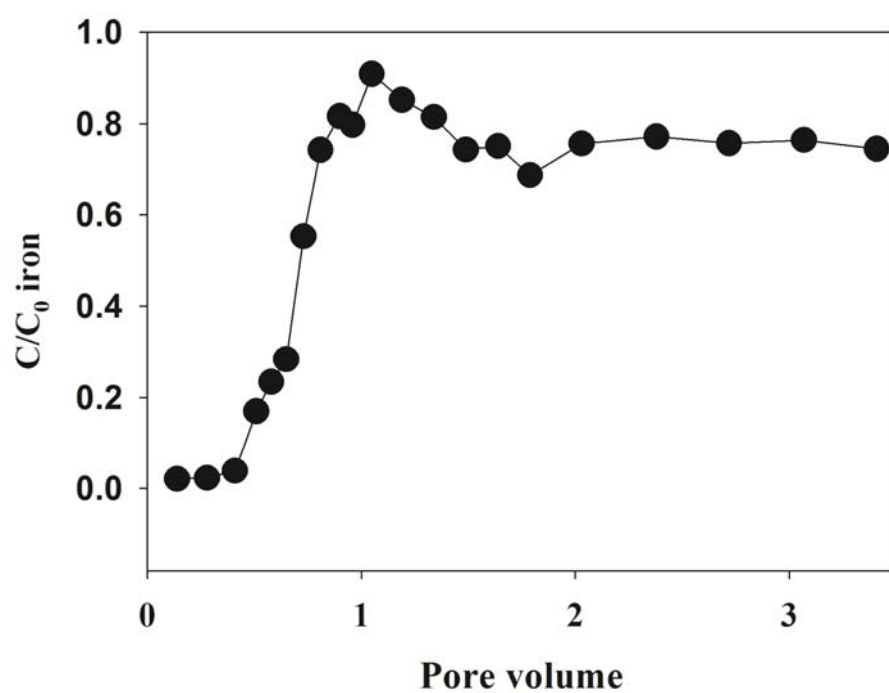

FIGURE S6. The eluted concentration of PAA modified NZVI from the soil column.
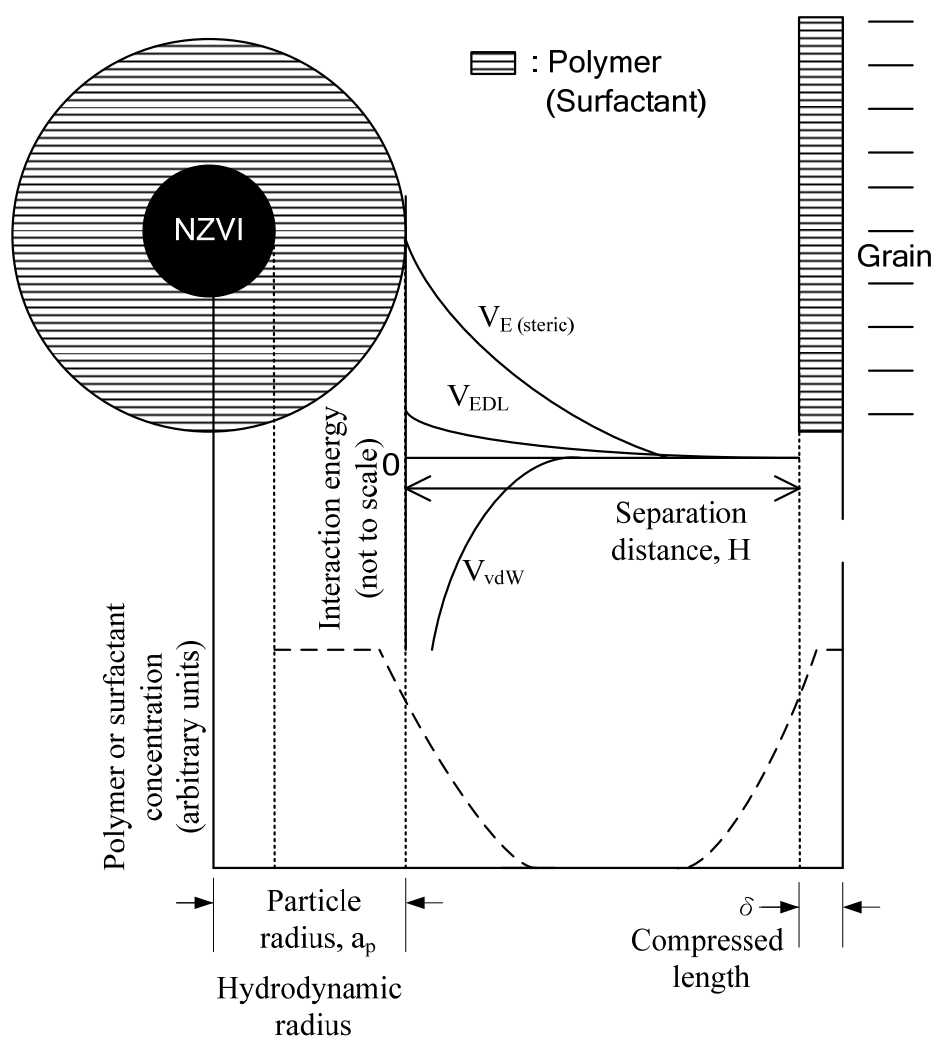
FIGURE S7. The simplified model adopted for calculating the total energy between polymer coated particle surface and collector surface.

Literature Cited

(1) Chow, J. C. F.; Soda, K. Laminar flow in tubes with constriction. *Phys. Fluids* **1972**, *15*, 1700–1706.

(2) Tien, C.; Ramarao, B. V. *Granular filtration of aerosols and hydrosols*; Elsevier: Oxford, 2007.

(3) Payatakes, A. C.; Tien, C.; Turian, R. M. A new model for granular porous media: Part I, model formulation. *AIChE J.* **1973**, *19* (1), 58–67.

(4) Elimelech, M. Particle deposition on ideal collectors from dilute flowing suspensions: mathematical formulation, numerical solution, and simulations. *Sep. Technol.* **1994.** *4*, 186–212.

(5) Adamczyk, Z.; Warszyński, P.; Szyk-Warszyńska L.; Weroński, P. Role of convection in particle deposition at solid surfaces. *Colloids Surf A Physicochem Eng Asp.* **2000**, *165*, 157–187.

(6) Nelson, K. E.; Ginn, T. R. Colloid filtration theory and the happel sphere-in-cell model revisited with direct numerical simulation of colloids. *Langmuir* **2005**, *21* (6), 2173–2184.

(7) Che, C.H. Preparation of nanoscale zero-valent iron suspension and its transport model in saturated soil layer, Master Thesis, National Taiwan University, Taiwan, 2008.

(8) Schrick, B.; Hydutsky, B. W.; Blough, J. L.; Mallouk, T. E. Delivery vehicles for zerovalent metal nanoparticles in soil and groundwater. *Chem. Mater* **2004**, *16*, 2187–2193.

(9) Phenrat, T.; Kim, H. J.; Fagerlund, F.; Illangasekare, T.; Tilton, R. D.; Lowry, G. V., Particle size distribution, concentration, and magnetic attraction affect transport of polymer-modified Fe0 nanoparticles in sand columns. *Environ. Sci. Technol.* **2009**, *43* (13), 5079–5085.

(10) Phenrat, T.; Saleh, N.; Sirk, K.; Kim, H.-J.; Tilton, R. D.; Lowry, G. V. Stabilization of aqueous nanoscale zerovalent iron dispersions by anionic polyelectrolytes: adsorbed anionic polyelectrolyte layer properties and their effect on aggregation and sedimentation *J. Nanopart. Res.* **2008**, *10*, 795–814.

(11) Runkana, V.; Somasundaran, P.; Kapur, P.C. Mathematical modeling of polymer-induced flocculation by charge neutralization. *J. Colloid Interface Sci.* **2004**, *270* (2), 347–358.

(12) Tadmor, R.; Rosensweig, R.E.; Frey, J.; Klein, J. Resolving the puzzle of ferrofluid dispersants. *Langmuir* **2000**, *16*(24), 9117–9120.

(13) Bell, N. S.; Sindel, J.; Aldinger, F.; Sigmund, W. M. Cation-induced collapse of low-molecular-weight polyacrylic acid in the dispersion of barium titanate *J. Colloid Interface Sci.* **2002**, *254*, 296–305.

(14) Russell, L.L., Chemical aspects of groundwater recharge with wastewaters, Ph.D. Thesis, University of California, Berkeley, USA, 1976

(15) Wei, Y. T.; Wu, S. C.; Chou, C. M.,; Che, C. H.; Tsai, S. M.; Lien, H. L. Influence of nanoscale zero-valent iron on geochemical properties of groundwater and vinyl chloride degradation: a field case study. *Water Res.* **2010**, *44* (1), 131–140.

(16) Ohshima, H. Electrophoretic mobility of soft particles. *Colloids Surf., A* **1995**, *103* (3), 249–255.

(17) Goodwin, J. *Colloids and interfaces with surfactants and polymers: An introduction*; John Wiley & Sons Ltd: Chichester, UK, 2004.